Propeller-Wing Interaction Using a Frequency Domain Panel Method

Jinsoo Cho* and Marc H. Williams†
Purdue University, West Lafayette, Indiana 47907

The unsteady aerodynamic coupling between a propeller and a wing is analyzed using linear compressible aerodynamic theory. The periodic loads are decomposed into harmonics, and the harmonic amplitudes are found iteratively. Each stage of the iteration involves the solution of an isolated propeller or wing problem; the interaction is done through the Fourier transform of the induced velocity field. The method was validated by comparing the predicted velocity field about an isolated propeller with detailed laser Doppler velocimeter measurements and by comparison with mean loads measured in a wing-propeller experiment. Comparisons have also been made between the fluctuating loads predicted by the present method and a quasisteady vortex lattice scheme.

Introduction

LINEARIZED frequency domain aerodynamic analysis is routinely used to predict fluctuating forces resulting from small amplitude vibrations and gusts on fixed wing aircraft. Such methods have also been used for isolated rotors. In this paper we present a frequency domain analysis applicable to systems with relative rotation in which there are multiple coupled harmonics. The method has been applied to a wing/propeller system. Mean and unsteady load results will be shown with comparisons to experimental data and a quasisteady calculation.

Several studies have been made of the effect of the propeller slipstream on wing performance using a variety of slipstream models. Kleinstein[1] treated the slipstream as a simple circular jet. Loth[2] added rigid rotation. Miranda[3] used a more realistic vortex tube model of the slipstream. In all three studies, the propwash field was prescribed, and the wing performance was obtained from lifting line theory. In contrast, Kroo[4] examined the optimization of integrated performance using a relatively simple model of the interference between rotor and wing. He concluded that performance benefits from swirl recovery that are comparable to those in counter-rotation systems can be achieved.

Unsteady loads have been calculated by Rangwalla[5] using a time marched incompressible panel method with a free-wake model. A similar approach, but with a rigid-wake model, was used by Chen[6] for a counter-rotating propeller system. Recently, Lee[7] used a quasisteady vortex lattice method for wing-propeller interference. This scheme does predict the unsteady loads, but the neglect of spanwise vortex shedding, which is implicit in the quasisteady approximation, casts some doubt on the accuracy of the predicted fluctuations—particularly for the high reduced frequencies present on the wing.

The scheme used here is an extension of the lifting surface panel method developed by Williams[8-10] for the aerodynamic and aeroelastic analysis of single rotation propellers. In that application, the blade loading is represented by a single frequency. The extension to wing/propeller interference (or counter-rotating propellers) requires that the loads be represented with multiple harmonics, which interact through the induced velocity field. The counter-rotation problem has been examined in Refs. 16 and 19 using essentially the same method described in this paper.

The induced velocity field calculation has been validated by comparison to laser Doppler velocimeter (LDV) measurements taken by Sundar[11] around a single rotation propeller. Similar LDV data, for a different rotor, was reported by Lepicovski.[12] Alternative velocity field calculations for Sundar's configuration based on an Euler code and vortex lattice model have been done by Usab et al.[13]

The present propeller/wing interference calculation has been validated by comparisons to wind-tunnel measurements made by Witkowski[14] and to Lee's quasisteady vortex lattice analysis of the same configuration. Both analyses agree well with measured mean performance but show significant differences in unsteady amplitudes.

Methodology

Harmonic Coupling

The unsteady interaction between a wing and rotor can be expressed by a pair of linear relations between the instantaneous normal velocity V and pressure difference Δp on the respective lifting surfaces,

$$V_R = A_{RR} \cdot \Delta p_R + A_{RW} \cdot \Delta p_W \tag{1a}$$

$$V_W = A_{WR} \cdot \Delta p_R + A_{WW} \cdot \Delta p_W \tag{1b}$$

The coefficients A are linear integral space/time operators. The solution (for Δp) can clearly be decomposed into the sum of rotor driven ($V_W = 0$) and wing driven ($V_R = 0$) parts. For the flow driven by the rotor, we suppose that V_R is simple harmonic with frequency ω_0 and interblade phase lag $m\Delta\theta$. For the flow driven by the wing, we suppose that V_W is simple harmonic with frequency ω_0.

In either case, the periodicity of the interaction implies that the loads, Δp_{R_j} on the jth blade and Δp_W on the wing, can be expanded in harmonics

$$\Delta p_{R_j} = \sum_n P_{R_n} e^{i(\omega_0 + n\Omega)t - ij(n+m)\Delta\theta} \tag{2a}$$

Received June 22, 1988; revision received Sept. 19, 1988.

*Graduate Student; currently visiting Assistant Professor, School of Aeronautics and Astronautics. Student Member AIAA.

†Associate Professor, School of Aeronautics and Astronautics. Member AIAA.

$$\Delta p_W = \sum_n P_{W_n} e^{i[\omega_0 + (nN-m)\Omega]t} \tag{2b}$$

where Ω is the angular velocity of the rotor, and N is the number of rotor blades. For the wing-driven flow, the blade phasing is fixed by the interaction so that $m = 0$. If the wing and rotor are rigid and the rotor is at zero incidence (the case examined in this paper) then $\omega_0 = m = 0$. If the rotor is pitched, then $\omega_0 = \Omega$ and $m = 1$.

The objective is to compute the harmonic load coefficients P_{R_n} and P_{W_n} for given normal velocities V. If we substitute the expansions of Eqs. (2a) and (2b) into Eqs. (1a) and (1b) and separate harmonics, we get

$$\bar{A}_{RR}(\omega_0 + n\Omega, n+m) \cdot P_{R_n} = \bar{V}_{R_n} \tag{3a}$$

$$\bar{A}_{WW}[\omega_0 + (nN-m)\Omega] \cdot P_{W_n} = \bar{V}_{W_n} \tag{3b}$$

where $\bar{A}_{RR}(\omega, k)$ denotes the simple harmonic reference blade operator for frequency ω and interblade phase lag $k\Delta\theta$, and $\bar{A}_{WW}(\omega)$ denotes the wing operator for simple harmonic motion with frequncy ω. The quantities $\bar{V}$ are the complex harmonic amplitudes of the normal velocity on each surface modified by the induced velocity from the other surface. Given $\bar{V}$, Eqs. (3a) and (3b) represent separate simple harmonic problems for the rotor and wing. Of course the $\bar{V}$ is not given but depends in a complicated way on the loads in all harmonics.

Each load harmonic P_{R_n} on the rotor produces a velocity field which is simple harmonic in the rotor frame ($\bar{\theta}$),

$$\boldsymbol{u}_{R_n} = \boldsymbol{U}_{R_n}(\bar{\theta}) e^{i(\omega_0 + n\Omega)t} \tag{4}$$

where the complex amplitude is found by an integral over the reference blade,

$$\boldsymbol{U}_{R_n} = \int\int P_{R_n}(\boldsymbol{x}_0) \boldsymbol{K}_R(\boldsymbol{x}, \boldsymbol{x}_0)\, \mathrm{d}A_0 \tag{5}$$

Explicit expressions for the rotor kernel, $\boldsymbol{K}_R$, will be found in Ref. 8. Note that the rotor operator $\bar{A}_{RR}$ is simply the normal projection of Eq. (5) on the reference blade.

The velocity field of Eq. (4) can be Fourier expanded in $\bar{\theta}$ and transformed to the wing frame through $\theta = \bar{\theta} - \Omega t$

$$\boldsymbol{u}_{R_n}(\theta, t) = e^{i(\omega_0 + n\Omega)t} \sum_k \left[\boldsymbol{U}_{R_{nk}} e^{iK\theta} \right] e^{iK\Omega t} \tag{6}$$

where $K = kN - n - m$ and

$$\boldsymbol{U}_{R_{nk}} = \frac{1}{\Delta\theta} \int_0^{\Delta\theta} \boldsymbol{U}_{R_n}(\bar{\theta}) e^{i(n+m-kN)\bar{\theta}}\, \mathrm{d}\bar{\theta} \tag{7}$$

The velocity field $\boldsymbol{U}_{R_{nk}} e^{iK\theta}$ corresponds to the wing frame frequency $\omega_0 + (kN-m)\Omega$ and therefore contributes to the wing normal velocity $\bar{V}_{W_k}$ in Eqs. (3a) and (3b) an amount

$$\Delta \bar{V}_{W_k} = -\boldsymbol{n}_W \cdot \boldsymbol{U}_{R_{nk}} e^{iK\theta} \tag{8}$$

where $\boldsymbol{n}_W$ is the normal to the wing camber surface.

Similarly, each load harmonic P_{W_n} on the wing produces a velocity field which is simple harmonic in the wing frame,

$$\boldsymbol{u}_{W_n} = \boldsymbol{U}_{W_n}(\theta) e^{i[\omega_0 + (nN-m)\Omega]t} \tag{9}$$

where the complex amplitude is found by an integral over the wing,

$$\boldsymbol{U}_{W_n} = \int\int P_{W_n}(\boldsymbol{x}_0) \boldsymbol{K}_W(\boldsymbol{x}, \boldsymbol{x}_0)\, \mathrm{d}A_0 \tag{10}$$

Explicit expressions for the wing kernel $\boldsymbol{K}_W$ will be found in Ref. 15. Note that the wing operator $\bar{A}_{WW}$ is the normal projection of Eq. (10) on the wing. This velocity field, too, can be Fourier expanded in θ and transferred to the rotor frame

$$\boldsymbol{u}_{W_n} = \sum_k \left[\boldsymbol{U}_{W_{nk}} e^{iK\bar{\theta}} \right] e^{i[\omega_0 + (nN-m-k)\Omega]t} \tag{11}$$

where

$$\boldsymbol{U}_{W_{nk}} = \frac{1}{2\pi} \int_0^{2\pi} \boldsymbol{U}_{W_n}(\theta) e^{-ik\theta}\, \mathrm{d}\theta \tag{12}$$

The velocity field $\boldsymbol{U}_{W_{nk}} e^{ik\bar{\theta}}$ corresponds to the rotor frame frequency $\omega_0 + (nN-m-k)\Omega$ and interblade phase angle $-k\Delta\theta$. Therefore it contributes to the rotor normal velocity $\bar{V}_{R_l}$ with $l = nN - m - k$ in Eqs. (3a) and (3b). (Note that $l + m = -k$ modulo N; therefore the interblade phases match.) The incremental contribution is

$$\Delta \bar{V}_{R_l} = -\boldsymbol{n}_R \cdot \boldsymbol{U}_{W_{nk}} e^{ik\bar{\theta}} \tag{13}$$

where $\boldsymbol{n}_R$ is the reference blade normal.

It should be observed that the complex amplitudes $\boldsymbol{U}_{R_n}$ must be computed [from Eq. (5)] over the volume swept out by the wing in the rotor frame and $\boldsymbol{U}_{W_n}$ must be computed [from Eq. (10)] over the volume swept out by the rotor in the wing frame. This is the most time consuming part of the calculation and care must be taken to minimize the number of points at which the velocities are evaluated as well as the computational effort involved in each evaluation.

Iterative Scheme

The calculation is performed iteratively in the following sequence. For each rotor harmonic: 1) compute prop loads, 2) compute propwash field around wing, 3) Fourier decompose propwash, and 4) distribute Fourier components to wing normal velocity harmonics. For each wing harmonic: 5) compute wing loads, 6) compute wingwash field around prop, 7) Fourier decompose wingwash, and 8) distribute Fourier components to prop normal velocity harmonics. This sequence is repeated to convergence. On initial entry, which could be either step 1 or 5, the interaction is ignored, and only one harmonic load is computed.

Propeller and Wing Discretization

The load integral equations, Eqs. (3a) and (3b), are both solved with a panel discretization of Eq. (5) and Eq. (9) for rotor and wing, respectively. The rotor solution is a direct application of the single rotation scheme described in Refs. 8 and 15. The wing analysis is a modification of that scheme, which makes use of the two fold translational symmetry of the wing kernel function to minimize the number of function evaluations. Further details on the propeller and wing analysis appear in Ref. 16.

At the discrete level, the solution of Eqs. (3a) and (3b) involves the inversion of a large system of simultaneous linear equations. To avoid repetitive calculation, the inverse influence coefficient matrix for each harmonic can be computed once and stored. The load calculation in steps 1 and 5 of the iteration is then reduced to a matrix-vector multiplication.

Most of the results reported here were obtained using seven chordwise panels on both the wing and rotor. Roughly 12–15 radial rows were used on the rotor blade and about 30 spanwise on the wing (concentrated in the disk plane). These numbers are adequate to resolve the integrated loads within a few percent.

Results

Isolated Propeller Velocity Field

The velocity calculation was tested on an isolated propeller for which Sundar[11] has made detailed LDV measurements.

The experimental configuration, shown in Fig. 1, contains an axisymmetric centerbody and two blades. The blades are straight, constant chord, aspect ratio 3 with fixed pitch of 45.4 deg at 3/4 blade tip radius, NACA 0010 airfoil sections, and an essentially helical twist distribution. Further details will be found in Refs. 11, 13, and 17.

Measured and calculated performance characteristics are shown in Fig. 2. Skin friction was not included in the force calculation, which accounts for the excessively high efficiencies near windmill. The agreement is otherwise quite good—especially near peak efficiency. The moderate underprediction of efficiency at high power (despite the neglect of viscous drag) is thought to be caused by the rigid wake model used in the analysis. The advance ratio scale at the top of the figure indicates the values used in the analysis (which differ somewhat from the experimental values, as suggested by the differences in efficiency).

For advance ratio $J = 1.66$, which is near peak efficiency, velocities were calculated at 13 radial stations (from $r/R = 0.22$ to 1.067) in 3-deg circumferential increments over one blade passage at each of the axial stations shown in Fig. 1. The velocities induced by the centerbody were computed by a line source distribution along the axis, and the blade thickness was accounted for with a source distribution laid on the blade camber surface.

Circumferentially averaged velocities, excluding blade thickness and centerbody, are shown in Fig. 3. This shows the expected axial acceleration balanced by a radial inflow. The mean swirl is zero upstream and constant downstream from the rotor. This is a direct consequence of the linearized circumferential momentum equation. If a nonlinear wake model were used, allowing for wake contraction, the mean swirl would vary in the wake (though only slightly for the experimental situation examined here).

To see the blade thickness effect, velocities near the blade-tip leading and trailing edges are shown in Fig. 4. These points are far enough outboard that the centerbody has negligible influence. Blade thickness influence is significant upstream but barely visible at the downstream station $x/R = 0.267$. Further downstream, blade thickness effects (which decay as a dipole) are quite negligible.

The circumferential variation of velocity at two axial and three radial stations is shown in Figs. 5 and 6. These results are dominated by blade loading except for the thickness effect at $x/R = -0.167$ already noted and a slight shift in axial and radial velocity at $x/R = 1$ induced by the motor housing. Overall the calculations agree remarkably well with the measurements even near the tip vortex (cf. $x/R = r/R = 1$ in Fig. 6). The rigid wake model used does produce a systematic phase shift between measured and calculated velocity peaks as x/R increases. This effect would be much stronger at lower advance ratios (higher blade loading).

A global picture of the calculated velocity field (with blade loading only) is given by a series of crossflow vector plots in Fig. 7. Neglecting the center body makes the flow appear to penetrate the hub. The two-tip vortices are clearly visible. Beyond about $x/R = 0.666$, the velocity field freezes into a rigidly rotating pattern determined by wake vorticity. This effect is also indicated by the circumferential averages in Fig. 3.

The results obtained for the isolated propeller are generally superior to the vortex lattice results reported in Ref. 12 for the same case primarily because the present method is less sensitive to discretization. The Euler calculation also reported in Ref. 12 does capture nonlinear wake effects, which we miss, but suffers from excessive artificial dissipative losses because of the coarse grid used.

Figure 8 gives the harmonic decomposition of the tangential velocities at the downstream station $x/R = 1$ as a function of spanwise location. This result corresponds to the first-order wing upwash at the quarter chord in the wing-propeller calculation discussed in the next section. Note that the amplitudes decrease rapidly with increasing frequency ($n = 3$ corresponds to a 6Ω wing excitation). Based on this result, the wing-propeller interaction was truncated at the third harmonic.

Propeller-Wing Interaction

Results will be presented for the propeller-wing configuration shown in Fig. 9, which is based on experimental work by Witkowski.[14] The propeller is identical to the isolated rotor examined in the last section. The wing is rectangular and the aspect ratio is 8.25 with an NACA 0010 section. The wing and rotor are separately articulated and mounted so that the axis of rotation lies in the wing symmetry plane (at $\alpha = 0$ deg).

Wing and blade thickness are ignored in the calculations because of the relatively large separation between the two. The system is assumed to be symmetric about the wing midspan. In contrast, the experiment used a wall mounted semispan model, and Lee[7] used a full span wing with a single tip mounted rotor in his quasisteady vortex lattice simulation.

We will first examine some properties of the mean loading for which there are experimental data. The characteristic fea-

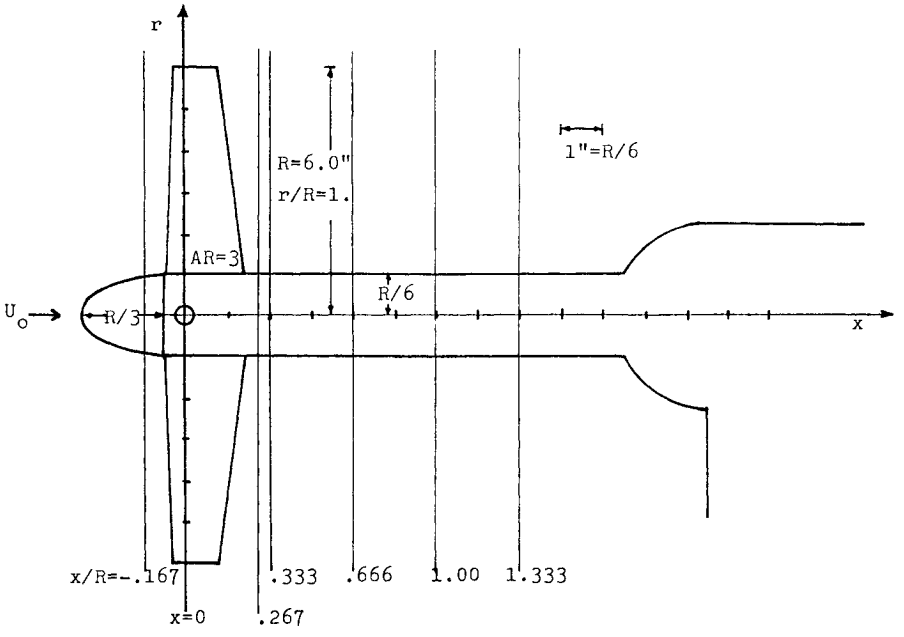

Fig. 1 Configuration of Sundar's experiment.

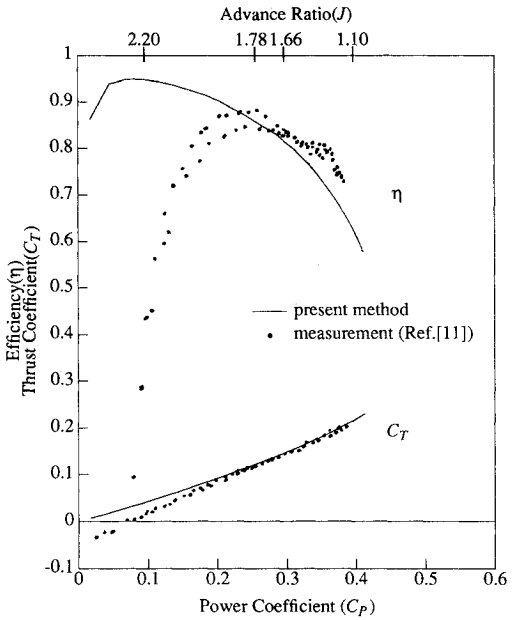

Fig. 2 Comparison of steady-state rotor performance parameters.

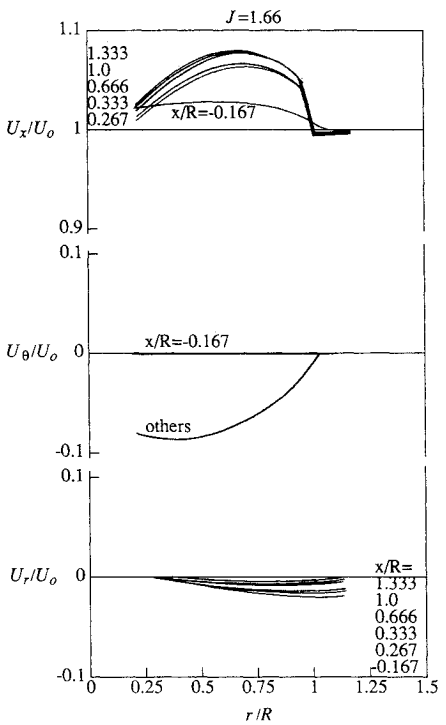

Fig. 3 Circumferentially averaged velocities.

tures of the unsteady fluctuations will then be described with comparisons to Lee's quasisteady analysis.

Figure 10 shows the effect of the propeller on the mean sectional lift distribution on the wing half span for a case where $\alpha = 8$ deg, $J = 1.66$. Three results are shown. The curve labeled "wing only" is the predicted load without propeller (the slight "wiggle" in the curve toward the tip is caused by the panel density which increases rapidly beyond $y/R = -1.50$). The dashed curve labeled "0th propwash" is the result of simply imposing the isolated propeller wake swirl (see Fig. 8) on the wing without accounting for the back influence of the wing on the rotor. Finally the solid curve shows the mean loading with complete interaction. Note that the effect of the prop effectively vanishes beyond one radius inboard from the inner tip. The effect of complete interaction is to slightly decrease the loads below the level set by the 0th propwash case, but the change is small. This figure can also be interpreted as

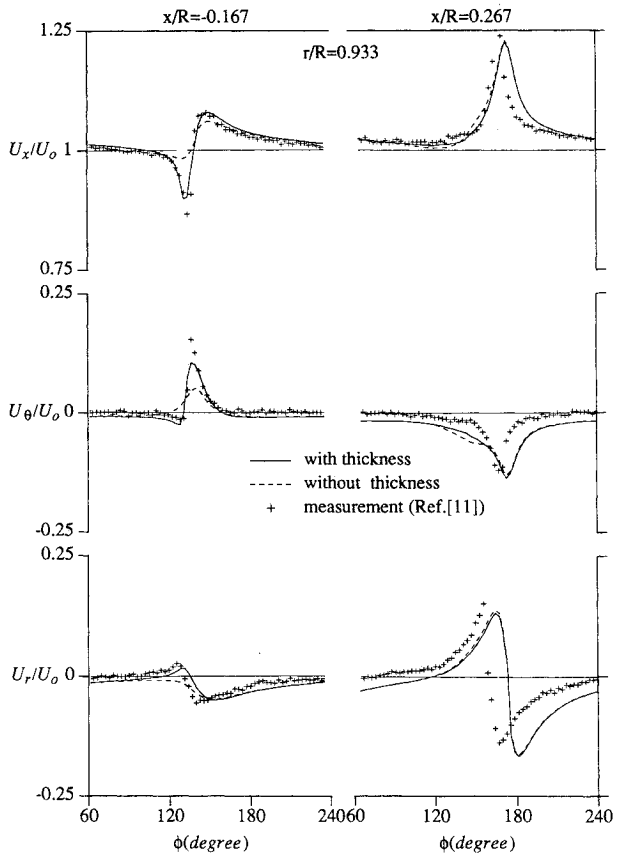

Fig. 4 Thickness effect near blade.

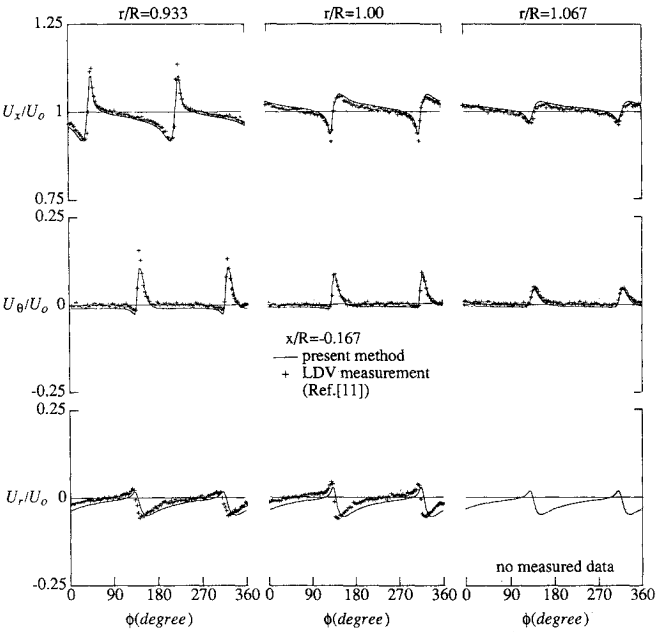

Fig. 5 Upstream velocity profiles ($x/R = -0.167$).

a convergence history of the iteration: the solid curve is reached after the first update of the prop loads, and further passes through the loop do not visibly alter the result. A similar comparison for the propeller is shown in Fig. 11. The curve labeled "0th wingwash" is the result of adding the isolated wingwash to the rotating propeller without accounting for the back influence of the propeller on the wing. There is practically no change in the mean thrust loading due to the interaction.

The total (time averaged) lift and drag on the wing as a function of angle of attack is shown in Figs. 12 and 13 with results from the present method, vortex lattice, and experiment. The calculations both agree remarkably well with the

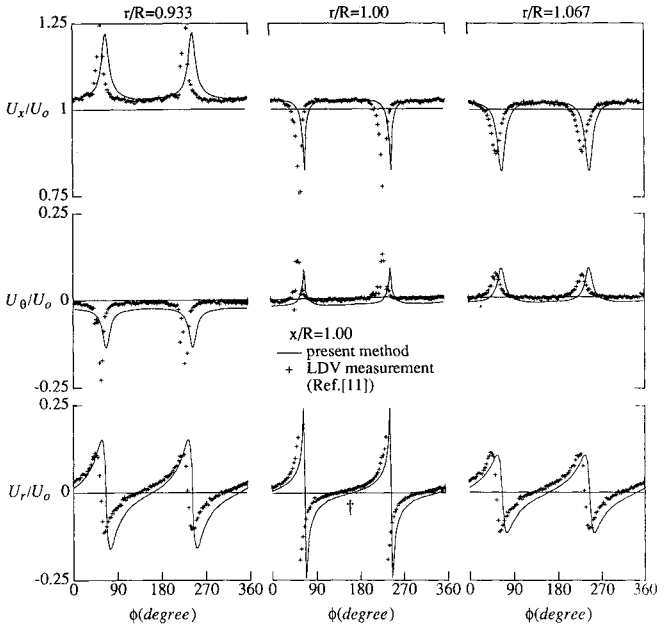

Fig. 6 Downstream velocity profiles ($x/R = 1$), (†vertical scale halved for clarity).

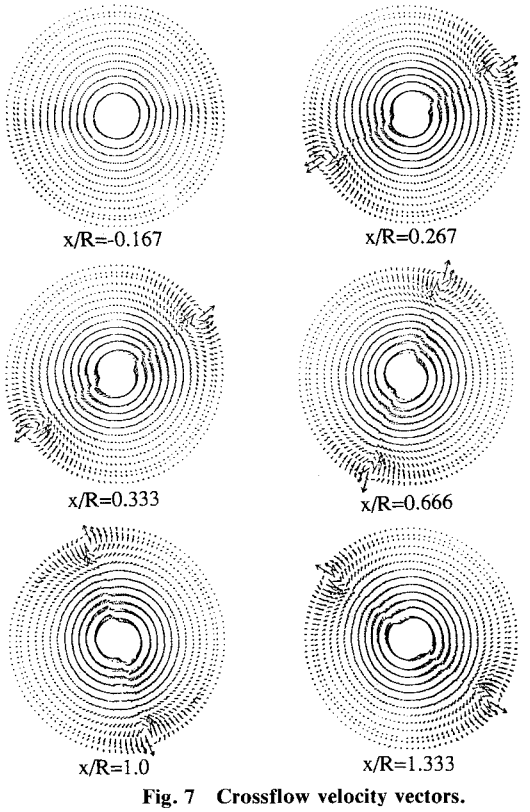

Fig. 7 Crossflow velocity vectors.

experiment apart from the expected roll off of the measured lift at a high angle of attack (the wing stalls around $\alpha = 14$ deg). The drag includes a viscous component (whose magnitude is estimated from sectional data in Ref. 18) as well as induced drag, which is indicated by the dotted line in Fig. 13. Note that the induced drag is slightly negative at low incidence reflecting the fact that the prop swirl actually induces thrust on the wing.

As mentioned in the Introduction, lift augmentation and drag reduction result from the propeller-wing interaction. This drag reduction is shown in Fig. 14. The ΔC_D is the difference between C_D of the interacting system and wing alone performance for the same value of C_L. The present unsteady result shows fairly good agreement with the quasisteady calculation and the experiment.

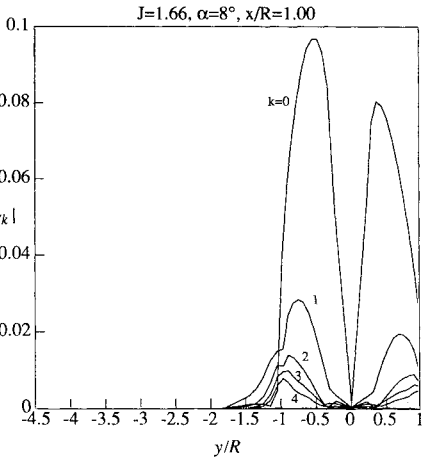

Fig. 8 Fourier decomposed propwash on wing.

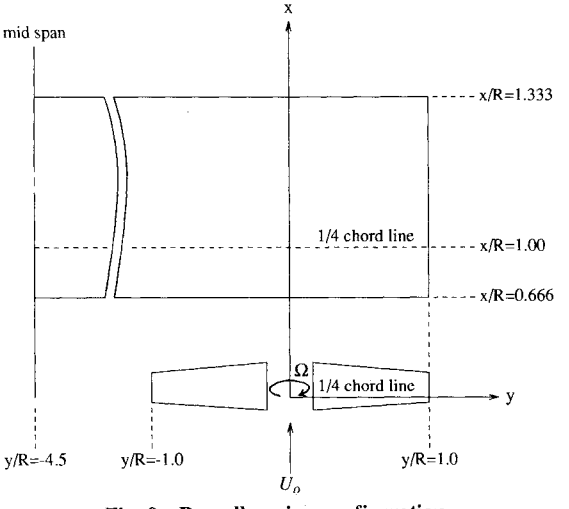

Fig. 9 Propeller-wing configuration.

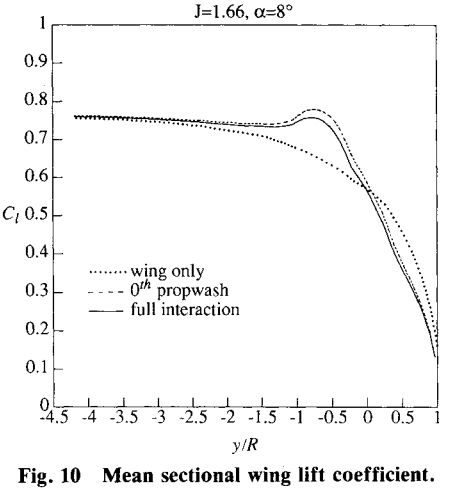

Fig. 10 Mean sectional wing lift coefficient.

Figure 15 shows the time history of wing sectional lift coefficient after propeller-wing interaction. Note that C_l is highest at around $\phi = 120$ deg when the propeller wake hits the quarter chord of the wing.

Figures 15–18 show unsteady load results on the wing and prop at two different advance ratios, $J = 1.66$ and 1.10 with comparisons to Lee's quasisteady analysis. The sectional thrust on the propeller at 3/4 blade-tip radius for $J = 1.66$ in Fig. 15 shows clearly that unsteady effects are not overly important here since the quasisteady and the unsteady analyses give basically the same time histories (the mean value offset

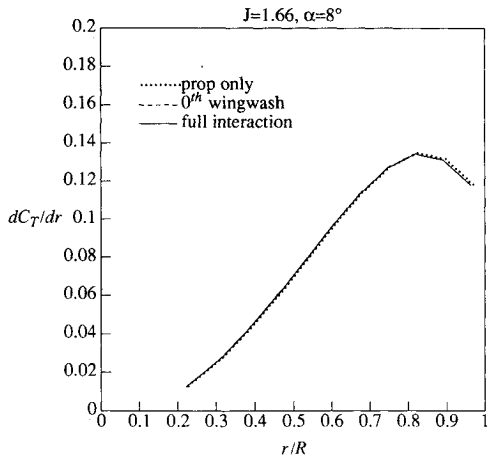

Fig. 11 Mean sectional thrust on propeller.

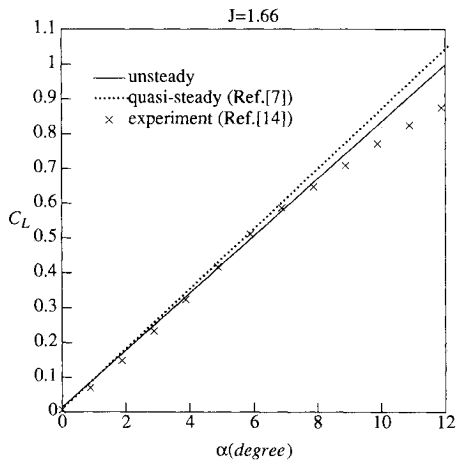

Fig. 12 Mean total wing lift.

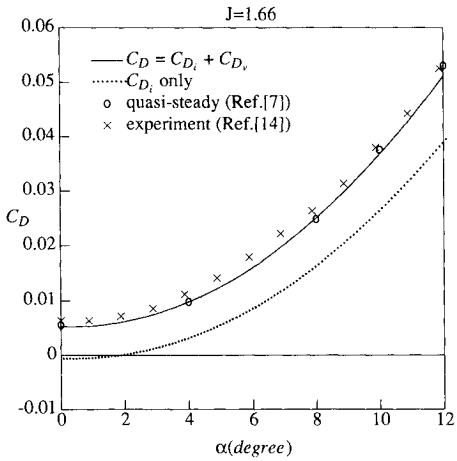

Fig. 13 Mean total wing drag.

between the two is discretization error as shown by the two "prop only" results). This agreement is understandable since the local reduced frequency k (based on Ω, prop chord, and relative velocity) is only 0.36.

In contrast, the time history of total lift on the wing for the same advance ratio shown in Fig. 16 shows large discrepancies between quasisteady and unsteady predictions. Here the fundamental reduced frequency is 5.05, which is far too large for a quasisteady approximation to be accurate. Also shown for reference is the isolated wing result. It is of interest to note that the zeroth propwash result shows higher mean lift than the full interaction does. This indicates that the prop-wing interaction decreases the mean C_L (which can be deduced from a two-dimensional model).

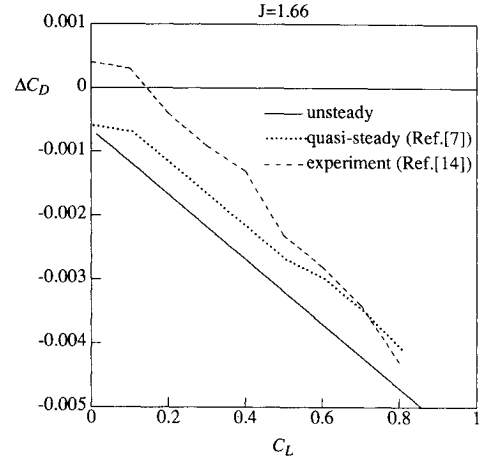

Fig. 14 Wing drag reduction by interaction.

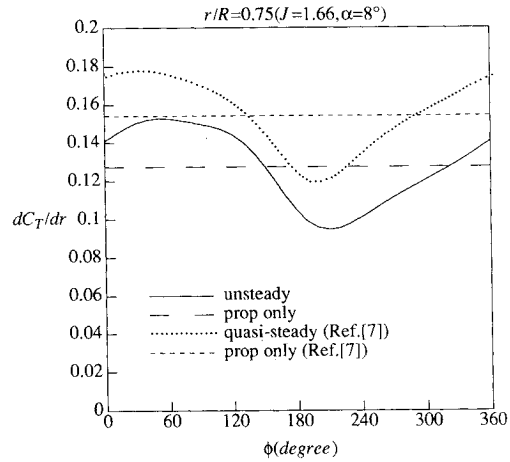

Fig. 15 Time history of blade sectional thrust for $J = 1.66$.

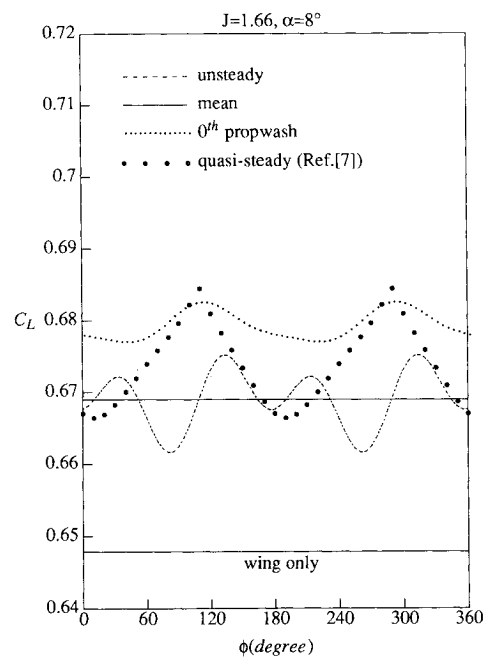

Fig. 16 Time history of wing lift for $J = 1.66$.

A spectral decomposition of the load time history (shown in Ref. 16) indicates that the basic wave form in Fig. 16 is set by the first three harmonics. Inclusion of more than three harmonics adds little but computational cost.

The situation for the more heavily loaded prop case, $J = 1.10$, is shown in Figs. 17–18. The sectional thrust loading

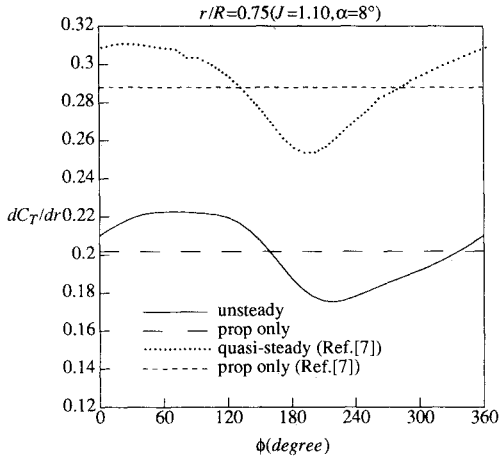

Fig. 17 Time history of blade sectional thrust for $J = 1.10$.

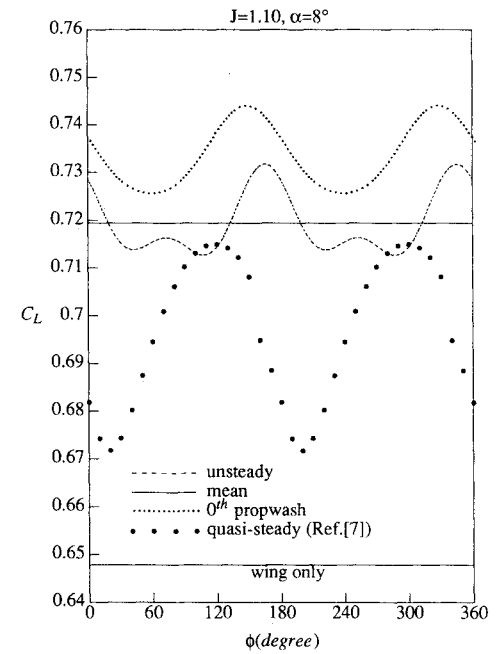

Fig. 18 Time history of wing lift for $J = 1.10$.

depicted in Fig. 17 is substantially similar to Fig. 15 largely because $k = 0.40$ is only slightly higher than it was. The quasisteady and unsteady time histories agree apart from the mean value shift, which is present even for the isolated rotor. However, the reduced frequency on the wing (based on the fundamental frequency of 2Ω) is now substantially greater (7.61) than it was at the higher advance ratio. Therefore the differences between the quasisteady and unsteady wing loads are greater as shown by comparing Fig. 18 with Fig. 16.

We believe that an aliasing problem occurs in the wing solution at reduced frequencies above 20 for the number of panels used in the $J = 1.66$ calculation (7 chordwise). The wavelength of the propwash for reduced frequency k and chord c is $2\pi c/k$ so that with 7 chordwise panels, there are fewer than two panels per wavelength when $k > 22$. Of course, this limit could be raised by increasing the number of panels. However, with any fixed numbers of panels, there will be an upper limit to the number of harmonics that can be retained (believably) using the present method. A more satisfactory solution to this problem would be to use an asymptotic high frequency approximation in place of the present panel method for the higher harmonics.

Conclusions

The lifting-surface method used here has been shown to predict excellent agreement with measured velocity field data for a single rotation propeller and generally good agreement with measured mean loads on a wing/propeller system. The unsteady load predictions agree with Lee's quasisteady analysis on the rotor where the reduced frequencies are relatively low but disagrees strongly on the wing where the reduced frequencies are high. Since the quasisteady approximation is only reasonable at low reduced frequencies, the present results on the wing are probably more accurate than Lee's. However, in the absence of experimental measurements or independent calculations of the unsteady loads, this statement must be viewed as a supposition. The present method is therefore preferable for forced vibration response applications but equivalent for performance predictions. (The computational cost is also roughly equivalent; though this depends on the number of panels and harmonics used in the present scheme and the number of vortex elements and time steps used in the vortex lattice method.)

The results of the prop-wing interaction analysis indicate that useful performance predictions can be made with a simplified model wherein the circumferentially averaged (isolated) propwash is imposed on the wing to get the modified steady-wing loading, and the circumferentially averaged (isolated) wingwash is imposed on the prop to get the modified steady-blade loading. All other interaction terms appear to have only a small effect on the mean performance. However, this conclusion may not hold for systems with smaller separation between the wing and rotor or higher prop loading than the case studied here.

It was found that for the cases examined, good estimates of the unsteady load fluctuations were obtained with just the first few harmonics. However, the panel method used can give poor results at extremely high frequencies. This becomes a serious problem when the propeller advance ratio decreases (higher RPM) and when the number of blades increases (high blade passage frequency). What is required is a better numerical scheme for evaluating high frequency response. Much more important, what is required is unsteady experimental data with which to compare.

Acknowledgment

The work reported here has been partially supported by NASA Lewis Research Center under Grant No. 3-499.

References

[1]Kleinstein, G., and Liu, C. H., "Application of Airfoil Theory for Nonuniform Streams to Wing Propeller Interaction," *Journal of Aircraft*, Vol. 9, No. 2, 1972, pp. 137-142.

[2]Loth, J. L., and Loth, F., "Induced Drag Reduction with Wing Tip Mounted Propellers," AIAA Paper 84-2149, Aug. 1984.

[3]Miranda, L. R., and Brennan, J. E., "Aerodynamic Effects of Wingtip-Mounted Propellers and Turbines," AIAA Paper 86-1802, Jan. 1986.

[4]Kroo, I., "Propeller-Wing Integration for Minimum Induced Loss," *Journal of Aircraft*, Vol. 23, No. 7, 1986, pp. 561-565.

[5]Rangwalla, A. A., and Wilson, L. N., "Application of a Panel Code to Unsteady Wing-Propeller Interference," *Journal of Aircraft*, Vol. 24, No. 8, 1987, pp. 568-571.

[6]Chen, S. H., "Panel Method for Counter Rotating Propellers," Ph.D. Dissertation, Purdue University, West Lafayette, IN, Dec. 1987.

[7]Lee, K. H., "A Computational Investigation of Propeller-Wing Interactions," M.S. Thesis, Purdue University, West Lafayette, IN, May 1988.

[8]Williams, M. H., "An Unsteady Lifting Surface Theory for Single Rotation Propellers," Purdue University, West Lafayette, IN, Rpt., June 1985.

[9]Williams, M. H., "User's Guide to UPROP3S," Purdue University, West Lafayette, IN, Rpt., Jan. 1985.

[10]Williams, M. H., and Hwang, C., "Three Dimensional Unsteady Aerodynamics and Aeroelastic Response of Advanced Turboprops," AIAA Paper 86-0846, May 1986.

[11]Sundar, R. M., "An Experimental Investigation of Propeller Wakes Using a Laser Doppler Velocimeter," Ph.D. Dissertation, Purdue University, West Lafayette, IN, May 1985.

[12]Lepicovsky, J., and Bell, W. A., "Aerodynamic Measurements About a Rotating Propeller with a Laser Velocimeter," *Journal of Aircraft*, Vol. 21, No. 4, 1984, pp. 264-271.

[13]Usab, W. J., Lee, K. H., and Sullivan, J. P., "A Comparison of Numerical Simulation and Experimental Measurements of Flow through Propellers," AIAA Paper 88-367, Jan. 1988.

[14]Witkowski, D. P., "Experimental Investigation of Propeller-Wing Interactions," M.S. Thesis, Purdue University, Aug. 1988.

[15]Bisplinghoff, R. L., and Ashley, H., *Principles of Aeroelasticity*, Wiley, New York, 1962.

[16]Cho, J., "Frequency Domain Aerodynamic Analysis of Interacting Rotating Systems," Ph.D. Thesis, Purdue University, Dec. 1988.

[17]Chang, L. K., "The Theoretical Performance of High Efficiency Propeller," Ph.D. Dissertation, Purdue University, West Lafayette, IN, Dec. 1980.

[18]Abbott, I. H., and Doenhoff, A. E., "Theory of Wing Sections, Including a Summary of Airfoil Data," Dover, New York, 1959.

[19]Cho, J., and Williams, M. H., "Counter-Rotating Propeller Analysis using a Frequency Domain Panel Method," *Journal of Propulsion and Power* (to be published).

Candidates Solicited for *JA* Editor-in-Chief Post

On January 1, 1991, AIAA will appoint an Editor-in-Chief of its *Journal of Aircraft (JA)* for a three-year term and solicits candidates for this prestigious editorial post.

Several goals have been established for *JA* beginning in FY'91:

- To serve the largest primary interest group of AIAA members—the field of aeronautics. Many of the technical areas listed in the scope (printed below) are not currently represented in the contents of the journal.
- To increase by 50% the number of papers published in *JA* by the end of FY'91 (with no reduction in quality).
- To make *JA* the first choice of submitting authors.
- To increase significantly the number of foreign papers published, particularly from Western Europe and Japan. The USSR is moving up quickly in many areas. Emphasis should be given to research that is more advanced than that in the United States.

We are soliciting applications for the Editor-in-Chief position because of these major changes in the goals for *JA*. The term of the current Editor-in-Chief, Thomas M. Weeks, expires on December 31, 1990. Dr. Weeks has been invited to apply.

The person recommended by the selection committee must convince them of his/her desire and ability to meet the goals outlined above.

The selection committee will be chaired by Allen E. Fuhs, former Vice President—Publications and *JA* Editor-in-Chief. Other members of the committee include Roy Lange, Daniel Raymer, and Charles Sprinkle.

To apply for the editorship, submit four copies of an application citing qualifications, your objectives for the journal, and how you will meet the above goals. Send them to

Dr. Allen E. Fuhs
c/o Norma J. Brennan
AIAA Headquarters
370 L'Enfant Promenade, S.W.
Washington, DC 20024-2518

*The deadline for applications is **June 1, 1990.*** The selection committee will recommend a candidate by August 1 for approval by the AIAA Board of Directors later in August.

JA now has the following scope:

"This Journal is devoted to the advancement of the science and technology of airborne flight through the dissemination of original archival papers describing significant advances in aircraft, the operation of aircraft, and applications of aircraft technology to other fields. The Journal publishes qualified papers on aircraft systems and advanced concepts in aircraft design, flight mechanics, flight testing; flight safety, weather hazards, human factors, airport design, airline operation; air traffic control; application of computers to aircraft; aircraft-oriented information systems; production methods; engineering economic analyses; reliability, maintainability, and logistics support; the integration of propulsion and control systems into aircraft design and operations; aircraft aerodynamics, structural design, and testing. It covers papers on general aviation; military as well as civilian aircraft; ground-effect machines; STOL and V/STOL airplanes; and supersonic, transonic, and hypersonic airplanes. Papers also are sought which definitively review the results of recent technical work from the standpoint of practical engineering."

Duties of the Editor-in-Chief encompass the following: Foreseeing and stimulating major contributions to the journal, with assistance from Associate Editors and an Editorial Advisory Board; logging in, acknowledging, and appraising submitted manuscripts; checking their general quality, importance to the technical community, and compliance with editorial specifications; assigning them to Associate Editors for processing; arbitrating editorial disputes; tracking manuscripts and Associate Editor actions via computer.

The post carries an honorarium of $275 per month and reimbursement for certain allowable expenses.

Address questions about editing procedures or other factors connected with duties to Norma Brennan, AIAA Director, Editorial and Production Departments (202-646-7482).

Questions concerning policy may be directed to me in writing at the following address: Dr. Billy M. McCormac, AIAA Vice President—Publications, 91-01/B282, Lockheed R&DD, 3251 Hanover Street, Palo Alto, CA 94304.

B.M.M.